Swelling pressure in systems with Na-montmorillonite and neutral surfaces: a molecular dynamics study

Hsiao Y-W, Hedström M

Published version information

Citation: Hsiao Y-W, Hedström M. "Swelling pressure in systems with Na-montmorillonite and neutral surfaces: a molecular dynamics study." J. Phys. Chem. C., vol. 121, no. 47 (2017): 26414-26423.

DOI: 10.1021/acs.jpcc.7b09496

Swelling Pressure in Systems with Na-Montmorillonite and Neutral Surfaces: A Molecular Dynamics Study

Ya-Wen Hsiao[*]*† and Magnus Hedström‡*

†Scientific Computing Department, STFC Daresbury Laboratory, Keckwick Lane, Daresbury, Warrington WA4 4AD, U.K.

‡Clay Technology AB, Ideon Science Park, SE-223 70, Lund, Sweden

ABSTRACT

In the present work, we used molecular dynamics simulations to evaluate the distance between montmorillonite layers, and between montmorillonite and a neutral surface for a range of applied pressures as in an oedometer-like setup. The neutral surface was represented by a layer of pyrophyllite. Due to explicit water in the simulation, the resulting osmotic pressure and basal distance relationship differs from that of DLVO theory for both interlayer types. In agreement with experiment, basal distances change abruptly between hydration states at certain pressures. Within a given hydration state, the basal distances were found to vary with applied pressure also seen

[*] Corresponding Author Tel: +44 (0)1925 603190. E-mail: ya-wen.hsiao@stfc.ac.uk.

experimentally. For the pressure range in the study, we found that water adjacent to neutral surfaces has interlayer character. The hydration state of the interlayer between montmorillonite and the neutral surface was found to be either the same or one water layer less compared to the pure montmorillonite interlayer. Water densities in this region were determined and the results show no significant difference to bulk density as some other studies reported. We also looked into reswelling and found it occurred without hysteresis.

INTRODUCTION

Nuclear power plants have been around and provided energy since the 1950s. Initially the question of nuclear waste seemed in most countries a relatively distant problem. Now, however, the management and disposal of nuclear waste have become high-priority international concerns and growing activities of the International Atomic Energy Agency (IAEA).[1] Still, to date, no country has yet constructed a final repository for spent nuclear fuel. The technique or principle for solving this issue varies from country to country, depending on local conditions as well as attitudes. Several designs for high-level nuclear waste storage are based on using bentonite clay. For example, in the Swedish KBS-3 proposal, the spent nuclear fuel is to be placed in copper canisters surrounded by bentonite at a depth of ca 500 m in granitic bedrock.[2] One of the functions of the bentonite is to prevent corroding agents from reaching the copper canister. In order to do this, the bentonite must have a high montmorillonite content and a high dry density to ensure a low hydraulic conductivity so that only diffusion dominates transport to the canister. In the event of a canister failure, the transport of escaping radionuclides would also be governed by diffusion. Another important function of the bentonite is to diminish activity of sulfate-reducing bacteria in

the vicinity of the canister, as sulfide is a potential corrosive agent. It has been found that such bacteria are inactive if the osmotic pressure in the bentonite is higher than approximately 5 MPa.[3] These requirements have led to an intensive study of the swelling characteristics of compacted bentonite/montmorillonite.[4–8] Another motive for understanding the details of clay swelling is and has historically been oil and gas extraction. In shale formations, the uptake of water from the drilling fluid by smectite clays may cause borehole instability, and thus much effort have been made to inhibit clay swelling.[9–11]

The swelling of bentonite originates from the properties of smectite clay (usually dominated by montmorillonite). Montmorillonite and other dioctahedral smectites consist of approximately 1 nm thick aluminosilicate layers with lateral dimensions typically in the range of 50-500 nm. These so-called 2:1 clay layers are structurally similar to pyrophyllite and are made up of two tetrahedral silicon oxide sheets sandwiching an octahedral aluminum oxide sheet (Figure 1). While pyrophyllite is charge neutral, smectite clay layers have a permanent negative charge due to isomorphous substitutions of, e.g., Mg(II) for Al(III) in the octahedral sheet or Al(III) for Si(IV) in the tetrahedral sheets. This permanent charge is neutralized by exchangeable cations that reside in the interlayer space between clay layers. In contact with water, the high concentration of ions in the interlayer causes osmotic transport of water into the interlayer, leading to swelling in the case of unconfined clay and to the build-up of an osmotic pressure (swelling pressure) if the available volume is restricted

The initial swelling of montmorillonite progresses stepwise, producing one, two, three, or sometimes four fairly distinct layers of water molecules in the interlayer space. Experimentally, these hydration states can be identified by measuring the basal spacings at different water content using X-ray powder diffraction.[12] The water content can be controlled by varying the relative

humidity [13–15], salinity of clay dispersion,[16,17] or by adding the wanted amount of water.[18] For Na-montmorillonite, the basal spacings are in the range 11.5−12.5 Å for the monohydrate (1WL), 14.5-15.5 Å for the bihydrate (2WL), and 18-19 Å for tri-hydrated clay (3WL).[12–14,16] Similar basal spacings are found with Li^+, Mg^{2+}, and Ca^{2+} as counterions. K^+ and Cs^+ give quite different basal spacings, presumably because of their larger sizes and weaker tendency to hydrate. In the case of the KBS-3 nuclear waste storage, the montmorillonite surrounding the canisters will be a mixture of bi- and tri-hydrated interlayers (in the region of 35% 2WL and 65% 3WL) at full water saturation.

For Li- and Na-montmorillonite at large basal distances, predictions from the DLVO theory[19,20] agree fairly well with measured swelling pressures.[6,21] However, the DLVO theory is less accurate at short separations because there the molecular details of the solvent become important, which in the case of water gives an additional hydration force[22] not accounted for by DLVO theory. Therefore, to give a realistic picture of compacted montmorillonite, atomistic simulations with explicit water molecules are needed.[23–30]

Swelling pressure is only developed when the montmorillonite is in contact with an external aqueous solution. At equilibrium the swelling pressure restores the chemical potential of the interlayer water to that of the external reservoir.[31] To simulate this process one needs to use an open ensemble that allows water molecules to move between the reservoir and the interlayer. In the past, swelling phenomena in montmorillonite have been studied using grand canonical or grand isoshear Monte Carlo (MC) simulations.[23–30] These simulations rely on insertion and deletion of water molecules into the interlayer based on the chemical potential of the external water source. A different approach was taken by Sun et al.[32] In their work the clay system was immersed in a large

volume of water and molecular dynamics (MD) simulations was employed to study the expansion of two montmorillonite layers against a constraining spring force.

In the present study we also used MD simulations of a clay system connected to an explicit bulk solution. The approach taken to determine the swelling pressure is the MD equivalent to oedometer tests where clay is compressed or expanded under constant load and the change in volume is measured.[5]

In a KBS-3 type nuclear waste repository, the montmorillonite will make interfaces with neutral or low-charged components. These are accessory minerals in the bentonite, the metal canister, and the rock into which the bentonite and canisters are emplaced. It is important to understand the nature of such interfaces because of the need to predict the chemical evolution in the repository. Traditionally, chemical processes such as mineral transformations or metal corrosion have been analyzed with models entirely dependent on the presence of bulk-like water inside the bentonite[33,34] despite strong evidence that most, if not all, water is of interlayer type in compacted bentonite.[6,35–37] Shifting the focus to interlayer water may have large consequences for the prediction of chemical processes in structures involving bentonite because of the Donnan potential[31,38,39] which leads to, e.g., an enhancement of cation concentration including lowering of pH and a depletion of anions.

Thus, the main focus of this work is to investigate the nature of water between montmorillonite and neutral surfaces, and between montmorillonite layers. Specifically, we discuss the water-film thickness, hydrogen-bond pattern, and the interfacial-water density. To this end, we determine the swelling pressure for two types of interlayers: the one between two montmorillonite layers and the one between montmorillonite and a neutral surface. The Poisson-Boltzmann (PB) equation predicts that the distance between a charged and a neutral surface is precisely half of the distance

between two equally charged surfaces.[40] The DLVO theory, on the other hand, gives an even shorter distance between a neutral and a charged surface, as it includes van der Waals attraction on top of the PB repulsion. In fact, at small layer separations DLVO theory actually predicts a collapse of the neutral-to-charged interlayer as demonstrated below. The DLVO predictions were compared to all atom MD simulations of the two types of interlayers. For the MD simulations we concentrated on short layer separations since they are most relevant for the nuclear waste repository. It is also at short separations where the molecular nature of the solvent is crucial.

In addition to elucidating the behavior of clay next to a neutral surface, the simulations also provided the dependence of swelling pressure on basal distance, and the first estimate of the interlayer water density under constant load in an open ensemble. Moreover, the origin of swelling hysteresis was reexamined.

THEORY AND MODELS

Swelling pressure from DLVO theory.

We consider a negatively charged surface and a neutral surface separated by a distance h. The surfaces are assumed to be parallel and have infinite lateral dimensions. The charged surface is located at $z = 0$ and the neutral one at $z = h$. Here and in the subsequent MD simulations we assume that the system is free of salt. Thus, there are only counterions in the system which gives the following PB equation if we also assume that the system is homoionic[40]

$$\frac{d^2\phi}{dz^2} = \frac{Ze}{\epsilon_r\epsilon_o} C(h)\exp(-\frac{Ze\phi}{k_BT}), \quad (1)$$

where ϕ is the electrostatic potential, Z the valence of the counterions, e the elementary charge, ϵ_0 the permittivity of vacuum, ϵ_r the relative permittivity of the solvent (78.4 for water at 298 K),

$C(z)$ the counterion concentration at z, k_B Boltzmann's constant, and T the absolute temperature. Because of the simple geometry, the charged surface is fully neutralized at the neutral wall, thus

$$\left.\frac{d\phi}{dz}\right|_{z=h} = 0. \quad (2)$$

At the charged surface the boundary condition is

$$\left.\frac{d\phi}{dz}\right|_{z=0} = -\frac{\sigma}{\epsilon_r\epsilon_0}, \quad (3)$$

where σ denotes the surface charge density. These two boundary conditions, together with a reference point for the potential allow for solving the PB equation. Because there is no excess salt present, a convenient reference for the potential is $\phi(h) = 0$. Moreover, since there is no electrostatic interaction between the charged and the neutral surfaces, the PB pressure is simply the osmotic pressure originating from the counterion concentration at the neutral surface, $C(h)$. It is implicitly understood that the system has access to external bulk water. The pressure has an analytical solution[40]

$$P_{PB} = \frac{2(k_BT)^2\epsilon_r\epsilon_0}{(Ze)^2}\left(\frac{s}{h}\right)^2, \quad (4)$$

where $0 \le s < \pi/2$ is obtained by numerically solving

$$s\tan s = -\frac{Ze\sigma h}{2k_BT\epsilon_r\epsilon_0}. \quad (5)$$

Because of symmetry, Eq. (4) is also valid for two equally charged surfaces separated by a distance of $2h$. At the midplane ($z = h$) between the two charged surfaces the electric field is zero and the boundary condition Eq. (2) holds. Thus within the PB framework, the only force transmitted between two equally charged surfaces is the osmotic pressure from the counterion concentration at the neutral plane (midplane). Consequently, at the level of PB theory the distance between a charged and a neutral surface is half of the distance between two charged surfaces, for any given pressure.

In DLVO theory the pressure is computed by adding the van der Waals attraction to Eq. (4). For two parallel surfaces of thickness δ separated by a distance h_s the non-retarded van der Waals pressure is given by[41]

$$P_{vdW} = -\frac{A_H}{6\pi}\left(\frac{1}{h_s^3} + \frac{1}{(h_s+2\delta)^3} - \frac{2}{(h_s+\delta)^3}\right) \qquad (6)$$

where A_H the effective Hamaker constant. Here, as well as in the subsequent MD simulations, the neutral surface is represented by a pyrophyllite (Py) layer, which we assume has the same thickness as montmorillonite (Mt). We also assume that A_H is the same between Py and Mt as between Mt and Mt. Note that when combining Eq. (6) with Eq. (4) to calculate the DLVO pressure, $h_s = h$ in case of Py-Mt and $h_s = 2h$ for Mt-Mt. Thus the van der Waals attraction is larger in the Py-Mt, than in the Mt-Mt system, implying that the separation between Py and Mt would be less than half of the separation between Mt and Mt at the same equilibrium pressure.

Figure 2 shows the calculated DLVO pressures for the Py-Mt and Mt-Mt systems, with monovalent counterions, $Z = 1$. We have used a representative surface charge density for Mt, $\sigma^{-1} = 140$ Å$^2/e$, and for both Py and Mt: $\delta = 9.3$ Å and $A_H = 2.2 \cdot 10^{-20}$ J. For $h > 20$ Å the contribution from Eq. (6) is relatively small so the pressure is governed by P_{PB} and thus the Py-Mt and the Mt-Mt pressures coincide (Figure 2). For shorter distances, the two pressure curves differ more and more as h decreases. At $h = 12$ Å the Py-Mt pressure reaches a maximum of 560 kPa. Consequently, for pressures above this value, an Mt-Mt system can only be in equilibrium with a Py-Mt system if all water leaves the Py-Mt interlayer. The pressure curve for Mt-Mt in Figure 2, also shows a maximum ($h = 3.8$ Å) and falls steeply at shorter distances, even giving negative pressures. Both features are in contradiction to experimental results that suggest an exponential increase in pressure with decreasing layer separation.[6,7,22,42] This discrepancy most probably reflect the omission of the hydration force.[43,44] Thus, the DLVO theory is not applicable to even qualitatively assess the

conditions that will prevail in the proposed nuclear waste repositories. MD simulations with explicit water molecules is one way to circumvent the shortcomings of DLVO and will be explored in the next section.

Swelling pressure from MD simulations.

The swelling pressure is established in the montmorillonite in order to equilibrate the internal water chemical potential with that of the external bulk solution. In this work we used pure water as external bulk. Thus the only ions in the system were the counterions balancing the structural charge in the clay. For our attempt to investigate the swelling/hydration behavior of montmorillonite in contact with an uncharged surface, a pyrophyllite layer (unit cell formula $Si_8Al_4O_{20}(OH)_4$) is employed to represent the uncharged surface. The atomic coordinates in the pyrophyllite layer were taken from Skipper et al.[45] and the same coordinates were used for the montmorillonite layers. Both pyrophyllite and montmorillonite were assumed to be rigid bodies. The lateral dimensions of the mineral layer unit cell are 5.28×9.14 $Å^2$ and each mineral layer in the simulation (two Mt and one Py) consisted of 32 unit cells in an 8×4 arrangement.

Partial charges and Lennard-Jones (LJ) parameters for mineral layers and counterions (Na^+) were taken from the CLAYFF force field.[46] The structural charge of the montmorillonite layer was -0.75e per $O_{20}(OH)_4$ formula unit and evenly distributed over all octahedrally coordinated Al atoms as in our previous study.[47] The mineral layers were terminated with -OH and $–OH_2$ groups at the interface with the explicit bulk water solution. The LJ parameters for these groups were the same as for the corresponding elements in CLAYFF, while the partial charges were adjusted based on Mulliken populations from DFT calculations.[47] Water was represented with the SPC/E model[48] and kept rigid using the SHAKE algorithm.[49]

A schematic of the simulation setup is shown in Figure 3. Initially both the pyrophyllite to montmorillonite basal distance d_{PM} and the montmorillonite to montmorillonite basal distance d_{MM} were set to 18.8 Å corresponding to a typical 3WL state. The mineral layers were free to move in the z-direction but tethered at x- and y-directions (tethering force constant: 10 kcal/(mol·Å)). Forces were applied in the z-direction both to the top montmorillonite layer and to the pyrophyllite layer at the bottom. With the knowledge of the layer surface area, the applied forces can be converted to pressure, P. During each simulation the applied pressure was kept constant and the basal distances d_{PM} and d_{MM} were recorded. Water molecules were allowed to move between the interlayers and the external reservoir. The simulation cell is large enough to also contain a vapor phase. Thus when water is squeezed out of the interlayers it will not increase the pressure of the bulk liquid. Instead, such water will be in equilibrium with its vapor. Additionally, this setup does not impose any particular partial molar volume of the interlayer water.

The simulations were carried out with the LAMMPS molecular dynamics program[50] in the NVT ensemble at 300 K and the equations of motion were integrated using a 2 fs time step. A cutoff radius of 10 Å was applied to short-range interactions and long-range Coulomb interactions were done using Particle–Particle-Particle–Mesh (PPPM) Ewald summation. The size of the simulation cell was 42.24×167.4×56.4 Å^3. The lateral size of the mineral layers was 42.24×36.56 Å^2 which is four times larger than in previous studies on clay swelling.[23–30,32] On each side of the mineral layers there was approximately 15 Å of bulk water along the y-direction (Figure 3). Both the larger lateral dimensions and the explicit contact of interlayer water to bulk water imply less constraints on the possible configurations that the interlayer water molecules may explore, which enables sampling of a larger volume of phase space in the simulations compared to earlier work.

RESULTS AND DISCUSSION

Swelling pressure.

As stated above, both basal distances d_{PM} and d_{MM} were initially set to 18.8 Å, corresponding to 3WL. After equilibration with the mineral layers kept fixed, a constant load was applied (z-direction) and the mineral layers were free to respond. Figure 4 shows the time evolution of d_{PM} and d_{MM} at four different loads: 14, 84, 210, and 280 MPa. At 14 MPa there is a transition from 3WL to 2WL in the Py-Mt interlayer after 8 ns; d_{PM} changes from 19 to 16.5 Å in a short time interval <1 ns. The Mt-Mt interlayer, having a larger amount of Na^+, withstands the 14 MPa load and remains in the 3WL. The basal distance d_{MM} is somewhat reduced and fluctuates around 18.5 Å. Thus at 14 MPa, the 3WL Mt-Mt interlayer is in equilibrium with a 2WL Py-Mt interlayer. With an increased load to 84 MPa the 3WL to 2WL transition follows rapidly (within 0.8 ns) for both Py-Mt and Mt-Mt. After a few more ns there is a further 2WL to 1WL transition for Py-Mt while Mt-Mt remains in the 2WL state. This is also the lowest applied pressure where the 2WL to 1WL transition was observed in Py-Mt. For pressures between 17 to 70 MPa, both interlayers are in the 2WL state as can be seen in Figure 5. Above 84 MPa, the Mt-Mt interlayer remains in the 2WL state up to an applied pressure of 196 MPa. At 210 MPa and above both interlayers are in the 1WL state (Figures 4 and 5). The pressures, where transitions from one hydration state to another take place, and the corresponding hydration states and distances are summarized in

Table 1.

Figure 5 shows the variation of mean basal distance with applied pressure. The error bars show the root-mean-square deviations evaluated from the fluctuations in basal distances at the respective equilibrium hydration states. We begin by discussing the Mt-Mt curve. The calculated swelling pressures for montmorillonite are a factor of two to three higher than experimental findings. For Wyoming montmorillonite the measured swelling pressure at a clay volume fraction corresponding to a 3WL state is approximately 5 MPa,[6,7] while our calculations predict the 3WL to 2WL transition to occur near 15 MPa. According to our data (Figure 5), the transition occurs at pressures between 14 and 16.8 MPa. However, given the large fluctuations in d_{MM} shown in Figure 4, it is reasonable to suggest that 14 MPa is very close to the pressure where the 3WL to 2WL transition occurs for Mt-Mt. When comparing to experiment, it should be pointed out however, that the experimental data were not obtained under compression with constant load but under constant volume where a given amount of clay adsorbs water via filters and the swelling pressure build-up is measured. The measured pressure eventually reaches a plateau, which is interpreted as the equilibrium pressure.[6,7] In experiments there is always a hysteresis present: pressures measured under compression are larger than pressures measured under expansion. In a constant-volume test, both compression and expansion may take place during the water-saturation phase. The final stable pressure is somewhere in between the extrema on the hysteresis curve.

The next transition, 2WL to 1WL, occurs around 200 MPa, where d_{MM} changes abruptly from 14.8 to 12.7 Å. For this transition there are no constant load pressure data but, the pressure at the transition can be deduced from desorption curves: Experimentally the 1WL in montmorillonite was observed when the relative humidity (RH) was reduced to 0.53 while it remained in the 2WL state at RH=0.64.[14] Assuming that the transition occurs between these RH values gives a

corresponding osmotic pressure of 74 MPa. Again the calculated pressure is a 2.7 times higher than the experimental value, consistent with our prediction for the 3WL to 2WL transition.

Although the pressures obtained in the simulation are larger than in experiments, they agree well with previous theoretical work. Simulations in the grand isoshear ensemble using TIP4P water predicted the 2WL to 1WL transition between RH 0.2 and 0.3, i.e., at 190 MPa.[11,25] Our results for the 3WL hydration state are also similar to the results of Sun et al.[32] although a comparison is not straightforward since their clay layer had a lower surface charge density, -0.5e/unit cell. Furthermore, because of their simulation model, basal distances show large fluctuations that encompasses more than one hydration state so information about specific transitions is somewhat lost.

Further, Figure 5 shows that for a given hydration state, the basal distance varies with applied pressure, which is in agreement with experiment.[12,14] Thus for the 2WL we find d_{MM} between 15.8 to 14.8 Å and for the 1WL, d_{MM}=12.7 Å at the transition and 12.6 Å at the highest applied load, 280 MPa.

Having tested the performance of our method for the Mt-Mt system, we now examine the Py-Mt system for which experimental data is lacking. Based on DLVO theory, the anticipated interlayer thickness would be less than half of that between two Mt layers. Therefore, it was somewhat unexpected to find that there are pressure intervals where both systems have the same hydration state (Figure 5). Furthermore, both for the 3WL and the 2WL states d_{PM} is even larger than the corresponding d_{MM}, in stark contrast to the DLVO theory. This stresses the importance of explicit water molecules, and that different surfaces organize water differently (see below). As can be seen in Figure 5 there are also pressure intervals where the Py-Mt system has one layer of water less than the Mt-Mt interlayer. For example, at 14 MPa, Mt-Mt is in the 3WL state, whereas the

transition to the 2WL state has occurred for Py-Mt: the transition to the 1WL state for Py-Mt is observed at 84 MPa, whereas Mt-Mt remains 2WL. The variation of basal distance with pressure within a given hydration state is also seen for Py-Mt. We also noted that d_{PM} is larger than d_{MM} where the 1WL first occur at 84 and 210 MPa, respectively. However, at 210 MPa, d_{MM} is larger than d_{PM} because of the continuous squeezing of the Py-Mt 1WL as the load increases from 84 to 210 MPa, while Mt-Mt has just undergone the 2WL to 1WL transition.

Pyrophyllite itself is a non-swelling mineral. This was also captured in scoping calculations using two pyrophyllite layers. When the initial state was 1WL, water left the interlayer without any applied force, most likely reflecting the strong van der Waals attraction between the two pyrophyllite layers. However, for basal distances larger than 16.5 Å the Py layers are separated by a distance that exceeds the short-range cutoff radius used in the simulations. Thus to induce the 3WL to 2WL transition we applied a pressure of 0.5 MPa, which is only about 5% of the pressure needed for the charged systems, Py-Mt and Mt-Mt. This demonstrates, within the accuracy of the method, that pressures obtained for the Py-Mt and Mt-Mt systems are due to the presence of surface charges and counterions.

As mentioned in the introduction, montmorillonite in the proposed KBS-3 type of repository for nuclear waste, will consist of roughly 35% 2WL and 65% 3WL. Thus under repository conditions, montmorillonite and neutral or low charged surfaces are separated by a 2WL (Figure 5). An important implication is that most of the water next to accessory minerals or the metal canister containing the spent fuel is of interlayer type and not bulk-like as hitherto has been assumed in geochemical modeling.[33,34] The chemical environment in interlayer water is different from a bulk solution and can be calculated through the use of the Donnan potential[31,38,39,47] and activity corrections.[51,52]

Interlayer structure.

Figure 6 shows the density profiles of interlayer water and Na^+ along the direction perpendicular to the clay layers. The applied load increases from the bottom to the top panel. All positions are measured relative to the central Mt layer. Due to fluctuations in basal distances, broadening of the profiles increases with distance from the reference plane. There is also a smearing effect (particularly for the central Mt layer at 14 MPa) due to small rotational motions of the clay layers since the tethering force is finite. Despite this broadening, the 3WL state is anyway discernible in the Mt-Mt interlayer at 14 MPa, showing two Na^+ peaks and three water oxygen peaks. On the Py-Mt side there is only one Na^+ peak and two oxygen peaks, signifying a 2WL. At all applied pressures, the most noticeable difference between the Py-Mt and the Mt-Mt interlayer density profiles is the missing water hydrogen peak next to the Py surface. There are occasionally hydrogens pointing towards the Py surface during the course of the simulation which give rise to the shoulder at the position of the "missing" peak. However, instead of making hydrogen bonds with the Py surface, most water molecules near Py form hydrogen bonds among themselves. This is most readily identified for the 2WL (14 and 56 MPa panels in Figure 6) where the hydrogen peak is almost twice as high as the oxygen peak, indicating that hydrogens and oxygens are located in the same plane. In all, this pattern is consistent with the notion of pyrophyllite being hydrophobic.[53] Whereas, next to the Mt surfaces, known to be hydrophilic,[54] hydrogen peaks between the siloxane oxygen (gray shaded in Figure 6) and the nearest water oxygen are always present, demonstrating the presence of hydrogen bonds to the surface.

Figure 6 suggests that Na^+ has a full first hydration shell in bi- and tri-hydrated interlayers, since the Na^+ density peak is located between water oxygen peaks. Thus the Na^+ distribution in the interlayer is to a large extent governed by hydration. Nevertheless, in the Py-Mt interlayer the

distribution of Na^+ is not symmetric but slightly shifted towards the charged Mt layer. In the 56 MPa panel the shift is about 0.5 Å. In the 1WL state there is no longer room for fully hydrated Na^+ and its peak coincides with the water oxygen peak. In the case of Mt-Mt both the oxygen and the Na^+ peaks are split (<1Å) suggesting that Na^+ also coordinates to siloxane oxygens on either side.

To further investigate the coordination of Na^+, the Na^+-O radial distribution function $g(r)$ was calculated and analyzed with respect to either water oxygen (O_{water}) or siloxane oxygens (O_{Py} or O_{Mt}). The coordination number was obtained by integrating $g(r)$ over the first peak and the results are shown in Figure 7. For the 3WL and 2WL states, Na^+ in the Mt-Mt interlayer is coordinated to 6.5 water oxygens, i.e., a full first hydration shell (upper panel, gray and yellow areas). In this configuration there is practically no Na^+ coordination to the surface oxygens. The same conclusion can be drawn for the Py-Mt interlayer (lower panel).

In the 1WL state of Mt-Mt, the total Na^+-O coordination number is reduced to six (upper panel of Figure 7, white area). On average, Na^+ is coordinated to 1.75 surface oxygens and 4.25 water oxygens. In the 1WL Py-Mt interlayer, Na^+ is coordinated to four water oxygens (slightly more than four at the lower pressure). Coordination of Na^+ to the charged Mt surface is favored over the neutral Py surface. However, the difference becomes smaller with increasing pressure.

Even at the highest pressures Na^+ is coordinated to four water oxygens, suggesting that the ions are not to any substantial extent occupying the siloxane hexagonal cavities. Representative structures for the Na^+ to oxygen coordination in the Py-Mt interlayer are shown in (Figure 8). The simulations indicate that the Na^+ coordination to the siloxane oxygens is asymmetric giving unequal bond lengths to the two surface oxygens.

Water content.

Our constant load approach allows for evaluating the water content at different pressures and therefore at different average basal distances. Figure 9 shows the average number of water molecules in the interlayer as a function of the average basal distance. The data are clustered in three groups reflecting the 1WL, 2WL, and 3WL states. The evaluated water content was based on water molecules with oxygen y–coordinates $\leq |10|$ Å. To our knowledge, this is the first molecular simulation relating the water content to the equilibrium basal distance obtained under constant applied pressure. Formally, one should evaluate the water partial molar volume. However, since all data points lie very close to the respective regression lines (R^2 >0.99 for both Py-Mt and Mt-Mt) one may actually evaluate a water density from the slope: 891 and 954 kg/m^3 for Py-Mt and Mt-Mt, respectively. Given the structuring influence of the surfaces and Na^+ on the water density profiles (Figure 6) it cannot be a priori postulated that the density of the interlayer water should be so close to that of the bulk. We are not aware of any measurements of the partial molar volume of montmorillonite interlayer water. However, there are reported evaluations of interlayer water density that hinge on the determination of the montmorillonite/bentonite grain density.[7] The current results support findings of the water density in bentonite being similar to that of bulk water.[4] Thus we may reject suggestions that the density of water in clay could be significantly higher (1200-1400 kg/m^3) than in bulk.[55,56]

Reswelling of compressed clay.

Experimental swelling pressure curves for smectite clays show hysteresis loops upon contraction and expansion: pressures measured under contraction are generally higher than pressures obtained under expansion.[4,42] Similarly, water retention at a given RH is higher upon desorption than adsorption.[12,14,57,58] MC simulations suggest that swelling hysteresis in montmorillonite stems from barriers between minima (corresponding to stable hydration states) in the swelling free

energy.[27,28] Free-energy barriers might be a plausible explanation for the swelling behavior at RH < 100%. However, for clay in contact with bulk water (same chemical potential as RH = 100%) the proposed barriers are so large that montmorillonite would not swell at all (see below), in contrast to experimental facts. For example, the barrier between 1WL and 2WL was estimated[27] to 3.4 k_BT/nm^2 and still higher values can be deduced from other MC calculations.[24,59] Even for the clay-layer size used in the present study, a barrier of 3.4 k_BT/nm^2 would amount to a total free-energy barrier of 53 k_BT, and thus completely prevent swelling.

To test this, we studied the reswelling of a system initially compressed by 210 MPa for 6 ns after which the load was reduced to 14 MPa. Figure 10 shows the time evolution of the basal distances d_{PM} and d_{MM}. With 210 MPa pressure, both Py-Mt and Mt-Mt rapidly reached the 1WL state. The reduction in pressure to 14 MPa resulted in an instantaneous response in both basal distances. In less than a nanosecond Mt-Mt had adsorbed a full hydration layer, while Py-Mt stayed in 1WL but with d_{PM} increased from 12.4 to 13 Å after <5 ns. The Mt-Mt system remained in the 2WL for 27 ns followed by a transition to 3WL, which is the equilibrium state found under compression by 14 MPa (Table 1). This finding is a manifestation of equilibrium behavior in the MD simulation; a given external pressure resulted in the same basal spacing regardless of whether the clay was expanding or being compressed. The fluctuations in d_{MM} for the 3WL state are also of similar magnitude as seen at 14 MPa is Figure 4. The reswelling from 1WL to 2WL and then from 2WL to 3WL occurred spontaneously and swiftly, indicating that the different hydration states are not separated by free-energy barriers. Therefore another explanation to swelling hysteresis must be sought.

In experiments, swelling pressure hysteresis is also observed at lower volume fractions, the so-called osmotic regime ($d_{MM} > 34$ Å), where the basal distance no longer shows jumps related to

water layers but varies continuously with water content.[4,42] Martin et al.[42] determined the equation of state for laponite clay (a synthetic hectorite with similar surface charge density as Mt) for volume fractions from 0.04 to almost 0.4 using ultracentrifugation. The water content of the clay at different positions in the centrifuge tube was analyzed and translated to volume fraction which was plotted against the centrifugal force (pressure) at each position. Hysteresis of up to a factor of four was observed between samples that have been compressed at high rotation speed and those that were reswelling at lower rotation speed. The authors suggested hydrodynamic drag forces and *internal friction* as possible candidates for the hysteresis. Furthermore, small angle neutron scattering on the compressed laponite (volume fractions from 0.09 to 0.31) revealed a strong structural organization. The clay layers were found to align with their normal along the axis of compression. Since there is no such thing as a one-dimensional crystal,[60] this alignment cannot be infinite. Thus, the degree of ordering may also contribute to the hysteresis. All of the above hypotheses for hysteresis reflect structures and processes beyond the interlayer and therefore beyond the scope of the present MD simulations.

There might still be a time asymmetry between swelling and deswelling as Py-Mt did not reach the anticipated 2WL during the 50 ns simulation shown in Figure 10. However, in the present study, the clay layers were kept rigid and not allowed to rotate. This means a severe restriction to the dynamics because the expansion from one hydration state to the next higher state only occurs if a there is a coordinated influx of water.[61] The transition in the Mt-Mt system from 1WL to 2WL involves the transfer of 150 water molecules from bulk to interlayer. From Figure 10 it is clear that the influx of water into the interlayer was rapid and took place immediately after the load was reduced to 14 MPa. Overall it took less than 1 ns and occurred in two steps. The initial water inflow

caused d_{MM} to increase to 14 Å and resulted in a precursor to a 2WL. After the formation of the precursor state, there was an almost instantaneous shift to the fully developed 2WL.

The 2WL to 3WL transition also occurs via precursor states. At 20 ns there was an influx of water that gave a temporary increase of d_{MM} from 16 to 17.7 Å. However, this state is only metastable and water will flow out unless this initial transition is followed by yet another coordinated water influx, hence the difference between the fluctuation at 20 ns and the completed expansion to the 3WL at 33-36 ns. For the layer size used in the simulation it means that approximately 150 water molecules have to flow from bulk to interlayer on the timescale of a few nanoseconds. The expansion of a realistic montmorillonite interlayer from one hydration state to the next requires approximately 500,000 water molecules, which seems prohibitive if the clay layers were rigid and always kept parallel. To our knowledge there has been no simulations in the open ensemble using flexible clay layers. However, a recent MD study in the NPT ensemble by Metz et al.[61] showed that fluctuations between two different solvation layers are possible within a single interlayer provided that the clay layers are flexible. The size of the undulation in their study was on the order of 30-50 Å which is comparable to the lateral dimensions of our rigid layers. This suggests that the hydration and dehydration of real clays may not need to involve 500,000 water molecules at once but a much smaller number, possibly of the order of 100, as in the present MD simulations. After the initial influx of a few hundred water molecules, the flexible clay layers facilitate a gradual expansion to propagate until the whole interlayer has reached the next hydration state.

CONCLUSIONS

We have presented the first MD simulation that mimics constant load oedometer experiments. Specific to our simulation method is the application of constant pressure to the clay layers, thereby determining the equilibrium basal distance as water equilibrates between the interlayer and an explicit bulk solution. The model consisted of three mineral layers, two montmorillonite and one pyrophyllite, which in the model represented a neutral surface. The equilibrium basal distances for both Mt-Mt and Py-Mt were determined simultaneously and in equilibrium with each other. Those basal distances change in a step-wise manner at pressures that are lower for the Py-Mt than the Mt-Mt system. Within a given hydration state the basal distances were found to vary with applied pressure in agreement with experiment.

The most important finding in this work is that the hydration state between montmorillonite and the neutral surface is either the same or one hydration layer less than in the Mt-Mt interlayer, depending on the applied pressure. As far as a nuclear waste repository is concerned a significant implication is that most water next to accessory minerals or the metal canister containing the spent fuel is of interlayer type. Thus, the modeling of corrosion and other chemical processes in this system so far based only on bulk-like water may be both irrelevant and possibly misleading.

The findings are also in contrast to both the DLVO theory that predicts the Py-Mt type of interlayer to collapse under the pressures used in this study (>4MPa), and PB theory which predicts the Py-Mt interlayer to be half as thick as the Mt-Mt interlayer. These differences are mainly a consequence of hydration forces and explicit water molecules present in the MD simulations. While DLVO predicts pressures too low for the Mt-Mt system at short basal distances compared to measured values, our MD simulations gives pressures about a factor of three too high, which is also similar to previously reported values from MC simulations.

We analyzed the interlayer water and Na^+ density profiles normal to the layers, at different swelling pressures/hydration states. Unsurprisingly, for the Mt-Mt type of interlayer the profiles were symmetric with respect to the midplane, while they were asymmetric for the Py-Mt. Na^+ was shifted towards the charged surface and next to the Py surface the water-hydrogen density peak was missing, indicating that water molecules next to Py prefer to form hydrogen bonds among themselves rather than to the hydrophobic Py. We also analyzed the coordination of Na^+ to oxygen. For 3WL and 2WL, Na^+ coordinates to 6.5 water molecules on average. Whereas, for the 1WL state Na^+ must coordinate to surface oxygens to fully coordinate, with a slight preference for Mt over Py.

The water content in the interlayer was determined and it varied linearly with basal distance both for Py-Mt and Mt-Mt. From the slope, the interlayer water density was evaluated. For both types of interlayers, it was below that of bulk water, 891 and 954 kg/m^3 for Py-Mt and Mt-Mt, respectively.

Allowing a compressed clay system to expand against a lower pressure we found that the Mt-Mt system returned to the same hydration state and basal distance as was obtained during compression under the same pressure. Thus, we found no basis for free-energy barriers separating the different hydration states. From our analysis we conclude that to explain swelling pressure hysteresis, structures and processes beyond the interlayer must be considered. Understanding of hysteresis in clay swelling is important and, based on our work, its origin needs to be readdressed.

ACKNOWLEDGMENTS

The authors thank Martin Birgersson, Dawn Geatches, Ola Karnland, and Sebastian Metz for valuable comments and suggestions on the manuscript.

REFERENCES

(1) Fischer, D. *History of the International Atomic Energy Agency: The First Forty Years*; International Atomic Energy Agency, 1997.

(2) SKB. *Long-Term Safety for the Final Repository for Spent Nuclear Fuel at Forsmark. Main Report of the SR-Site Project*; SKB Technical Report TR-11-01, 2011.

(3) Pedersen, K.; Motamedi, M.; Karnland, O.; Sandén, T. Mixing and Sulphate-Reducing Activity of Bacteria in Swelling, Compacted Bentonite Clay under High-Level Radioactive Waste Repository Conditions. *J. Appl. Microbiol.* **2000**, *89*, 1038–1047.

(4) Börgesson, L.; Hökmark, H.; Karnland, O. *Rheological Properties of Sodium Smectite Clay*; SKB Technical Report TR-88-30, 1988.

(5) Börgesson, L.; Johannesson, L.-E.; Sandén, T.; Hernelind, J. *Modelling of the Physical Behaviour of Water Saturated Clay Barriers. Laboratory Tests, Material Models and Finite Element Application*; SKB Technical Report TR-95-20, 1995.

(6) Karnland, O.; Muurinen, A.; Karlsson, F. Bentonite Swelling Pressure in NaCl Solutions - Experimentally Determined Data and Model Calculations. In *Advances in Understanding Engineered Clay Barriers*; Alonso, E. E., Ledesma, A., Eds.; Taylor & Francis Group, London, 2005; pp 241–256.

(7) Karnland, O.; Olsson, S.; Nilsson, U. *Mineralogy and Sealing Properties of Various Bentonites and Smectite-Rich Clay Material*; SKB Technical Report TR-06-30, 2006.

(8) Kahr, G.; Kraehenbuehl, F.; Stoeckli, H. F.; Mueller-Vonmoos, M. Study of the Water-Bentonite System by Vapour Adsorption, Immersion Calorimetry and X-Ray Techniques; II, Heats of Immersion, Swelling Pressures and Thermodynamic Properties. *Clay Miner.* **1990**, *25*, 499–506.

(9) Boek, E. S.; Coveney, P. V.; Skipper, N. T. Monte Carlo Molecular Modeling Studies of Hydrated Li-, Na-, and K-Smectites: Understanding the Role of Potassium as a Clay Swelling Inhibitor. *J. Am. Chem. Soc.* **1995**, *117*, 12608–12617.

(10) Anderson, R. L.; Ratcliffe, I.; Greenwell, H. C.; Williams, P. A.; Cliffe, S.; Coveney, P. V. Clay Swelling — A Challenge in the Oilfield. *Earth-Sci. Rev.* **2010**, *98*, 201–216.

(11) Odriozola, G.; Aguilar, J. F.; López-Lemus, J. Na-Montmorillonite Hydrates under Ethane Rich Reservoirs: $NP_{zz}T$ and $\mu P_{zz}T$ Simulations. *J. Chem. Phys.* **2004**, *121*, 4266–4275.

(12) *Crystal Structures of Clay Minerals and Their X-Ray Identification*; Brindley, G. W., Brown, G., Eds.; Mineralogical Society, 1980.

(13) Cases, J. M.; Berend, I.; Besson, G.; Francois, M.; Uriot, J. P.; Thomas, F.; Poirier, J. E. Mechanism of Adsorption and Desorption of Water Vapor by Homoionic Montmorillonite. 1. The Sodium-Exchanged Form. *Langmuir* **1992**, *8*, 2730–2739.

(14) Fu, M. H.; Zhang, Z. Z.; Low, P. F. Changes in the Properties of a Montmorillonite-Water System during the Adsorption and Desorption of Water: Hysteresis. *Clays Clay Miner.* **1990**, *38*, 485–492.

(15) Keren, R.; Shainberg, I. Water Vapor Isotherms and Heat of Immersion of Na/Ca-Montmorillonite Systems; I, Homoionic Clay. *Clays Clay Miner.* **1975**, *23*, 193–200.

(16) Norrish, K. The Swelling of Montmorillonite. *Discuss. Faraday Soc.* **1954**, *18*, 120–134.

(17) Slade, P.; Quirk, J. The Limited Crystalline Swelling of Smectites in $CaCl_2$, $MgCl_2$, and $LaCl_3$ Solutions. *J. Colloid Interface Sci.* **1991**, *144*, 18–26.

(18) Zhang, Z. Z.; Low, P. F. Relation between the Heat of Immersion and the Initial Water Content of Li-, Na-, and K-Montmorillonite. *J. Colloid Interface Sci.* **1989**, *133*, 461–472.
(19) Derjaguin, B.; Landau, L. Theory of the Stability of Strongly Charged Lyophobic Sols and of the Adhesion of Strongly Charged Particles in Solutions of Electrolytes. *Acta Phys. Chem. URSS* **1941**, *14*, 633–662.
(20) Verwey, E. J. W.; Overbeek, J. T. G. *Theory of the Stability of Lyophobic Colloids*; Dover, 1948.
(21) Quirk, J. P.; Marčelja, S. Application of Double-Layer Theories to the Extensive Crystalline Swelling of Li-Montmorillonite. *Langmuir* **1997**, *13*, 6241–6248.
(22) Pashley, R. M.; Israelachvili, J. N. Molecular Layering of Water in Thin Films between Mica Surfaces and Its Relation to Hydration Forces. *J. Colloid Interface Sci.* **1984**, *101*, 511–523.
(23) Chávez-Páez, M.; dePablo, L.; dePablo, J. J. Monte Carlo Simulations of Ca–montmorillonite Hydrates. *J. Chem. Phys.* **2001**, *114*, 10948–10953.
(24) Chávez-Páez, M.; Workum, K. V.; Pablo, L. de; Pablo, J. J. de. Monte Carlo Simulations of Wyoming Sodium Montmorillonite Hydrates. *J. Chem. Phys.* **2001**, *114*, 1405–1413.
(25) Hensen, E. J. M.; Smit, B. Why Clays Swell. *J. Phys. Chem. B* **2002**, *106*, 12664–12667.
(26) Shroll, R. M.; Smith, D. E. Molecular Dynamics Simulations in the Grand Canonical Ensemble: Application to Clay Mineral Swelling. *J. Chem. Phys.* **1999**, *111*, 9025–9033.
(27) Smith, D. E.; Wang, Y.; Chaturvedi, A.; Whitley, H. D. Molecular Simulations of the Pressure, Temperature, and Chemical Potential Dependencies of Clay Swelling. *J. Phys. Chem. B* **2006**, *110*, 20046–20054.
(28) Tambach, T. J.; Bolhuis, P. G.; Hensen, E. J. M.; Smit, B. Hysteresis in Clay Swelling Induced by Hydrogen Bonding: Accurate Prediction of Swelling States. *Langmuir* **2006**, *22*, 1223–1234.
(29) Tambach, T. J.; Hensen, E. J. M.; Smit, B. Molecular Simulations of Swelling Clay Minerals. *J. Phys. Chem. B* **2004**, *108*, 7586–7596.
(30) Whitley, H. D.; Smith, D. E. Free Energy, Energy, and Entropy of Swelling in Cs-, Na-, and Sr-Montmorillonite Clays. *J. Chem. Phys.* **2004**, *120*, 5387–95.
(31) Birgersson, M.; Hedström, M.; Karnland, O.; Sjöland, A. 12 - Bentonite Buffer: Macroscopic Performance from Nanoscale Properties. In *Geological Repository Systems for Safe Disposal of Spent Nuclear Fuels and Radioactive Waste (Second Edition)*; Woodhead Publishing Series in Energy; Woodhead Publishing, 2017; pp 319–364.
(32) Sun, L.; Hirvi, J. T.; Schatz, T.; Kasa, S.; Pakkanen, T. A. Estimation of Montmorillonite Swelling Pressure: A Molecular Dynamics Approach. *J. Phys. Chem. C* **2015**, *119*, 19863–19868.
(33) Sena, C.; Salas, J.; Arcos, D. *Aspects of Geochemical Evolution of the SKB near Field in the Frame of SR-Site*; SKB Technical Report TR-10-59, 2010.
(34) King, F.; Lilja, C.; Pedersen, K.; Pitkänen, P.; Vähänen, M. *An Update of the State-of-the-Art Report on the Corrosion of Copper under Expected Conditions in a Deep Geologic Repository*; SKB Technical Report TR-10-67, 2010.
(35) Birgersson, M.; Karnland, O.; Nilsson, U. Freezing in Saturated Bentonite – A Thermodynamic Approach. *Phys. Chem. Earth Parts ABC* **2008**, *33*, S527–S530.
(36) Glaus, M. A.; Baeyens, B.; Bradbury, M. H.; Jakob, A.; Van Loon, L. R.; Yaroshchuk, A. Diffusion of ^{22}Na and ^{85}Sr in Montmorillonite: Evidence of Interlayer Diffusion Being the Dominant Pathway at High Compaction. *Environ. Sci. Technol.* **2007**, *41*, 478–485.

(37) Glaus, M. A.; Birgersson, M.; Karnland, O.; Van Loon, L. R. Seeming Steady-State Uphill Diffusion of $^{22}Na^{+}$ in Compacted Montmorillonite. *Environ. Sci. Technol.* **2013**, *47*, 11522–11527.
(38) Donnan, F. G. The Theory of Membrane Equilibria. *Chem. Rev.* **1924**, *1*, 73–90.
(39) Mosslehi, M.; Lambrosa, A.; Marinsky, J. A. *The Interaction of Bentonite and Glass with Aqueous Media*; Technical Report; SKBF/KBS TR-83-33, 1983.
(40) Evans, D. F.; Wennerström, H. *The Colloidal Domain: Where Physics, Chemistry, Biology, and Technology Meet*, 2nd ed.; Wiley-VCH: New York, 1999.
(41) Russel, W. B.; Saville, D. A.; Schowalter, W. R. *Colloidal Dispersions*; Cambridge University Press, 1992.
(42) Martin, C.; Pignon, F.; Magnin, A.; Meireles, M.; Lelièvre, V.; Lindner, P.; Cabane, B. Osmotic Compression and Expansion of Highly Ordered Clay Dispersions. *Langmuir* **2006**, *22*, 4065–4075.
(43) Ruths, M.; Israelachvili, J. N. Surface Forces and Nanorheology of Molecularly Thin Films. In *Nanotribology and Nanomechanics*; Springer Berlin Heidelberg, 2008; pp 417–515.
(44) Marčelja, S.; Radić, N. Repulsion of Interfaces Due to Boundary Water. *Chem. Phys. Lett.* **1976**, *42*, 129–130.
(45) Skipper, N. T.; Chang, F.-R. C.; Sposito, G. Monte Carlo Simulation of Interlayer Molecular Structure in Swelling Clay Minerals; 1, Methodology. *Clays Clay Miner.* **1995**, *43*, 285–293.
(46) Cygan, R. T.; Liang, J.-J.; Kalinichev, A. G. Molecular Models of Hydroxide, Oxyhydroxide, and Clay Phases and the Development of a General Force Field. *J. Phys. Chem. B* **2004**, *108*, 1255–1266.
(47) Hsiao, Y.-W.; Hedström, M. Molecular Dynamics Simulations of NaCl Permeation in Bihydrated Montmorillonite Interlayer Nanopores. *J. Phys. Chem. C* **2015**, *119*, 17352–17361.
(48) Berendsen, H. J. C.; Grigera, J. R.; Straatsma, T. P. The Missing Term in Effective Pair Potentials. *J. Phys. Chem.* **1987**, *91*, 6269–6271.
(49) Ryckaert, J.-P.; Ciccotti, G.; Berendsen, H. J. C. Numerical Integration of the Cartesian Equations of Motion of a System with Constraints: Molecular Dynamics of n-Alkanes. *J. Comput. Phys.* **1977**, *23*, 327–341.
(50) Plimpton, S. Fast Parallel Algorithms for Short-Range Molecular Dynamics. *J. Comput. Phys.* **1995**, *117*, 1–19.
(51) Gregor, H. P. Gibbs-Donnan Equilibria in Ion Exchange Resin Systems. *J. Am. Chem. Soc.* **1951**, *73*, 642–650.
(52) Birgersson, M. A General Framework for Ion Equilibrium Calculations in Compacted Bentonite. *Geochim. Cosmochim. Acta* **2017**, *200*, 186–200.
(53) Giese, R. F.; Costanzo, P. M.; Oss, C. J. van. The Surface Free Energies of Talc and Pyrophyllite. *Phys. Chem. Miner.* **1991**, *17*, 611–616.
(54) van Oss, C. J.; Giese, R. F. The Hydrophilicity and Hydrophobicity of Clay Minerals. *Clays Clay Miner.* **1995**, *43*, 474–477.
(55) Jacinto, A. C.; Villar, M. V.; Ledesma, A. Influence of Water Density on the Water-Retention Curve of Expansive Clays. *Géotechnique* **2012**, *62*, 657–667.
(56) Villar, M. V.; Lloret, A. Influence of Temperature on the Hydro-Mechanical Behaviour of a Compacted Bentonite. *Appl. Clay Sci.* **2004**, *26*, 337–350.

(57) Dueck, A. Laboratory Results from Hydro-Mechanical Tests on a Water Unsaturated Bentonite. *Eng. Geol.* **2008**, *97*, 15–24.
(58) Dueck, A.; Nilsson, U. *Thermo-Hydro-Mechanical Properties of MX-80. Results from Advanced Laboratory Tests*; SKB Technical Report TR-10-55, 2010.
(59) Zhou, J.; Boek, E. S.; Zhu, J.; Lu, X.; Sprik, M.; He, H. Molecular Simulation Study of Hydrated Na-Rectorite. *Langmuir* **2015**, *31*, 2008–2013.
(60) Ziman, J. M. *Principles of the Theory of Solids*, 2nd ed.; Cambridge University Press: Cambridge, 1979.
(61) Metz, S.; Anderson, R. L.; Geatches, D. L.; Suter, J. L.; Lines, R.; Greenwell, H. C. Understanding the Swelling Behavior of Modified Nanoclay Filler Particles in Water and Ethanol. *J. Phys. Chem. C* **2015**, *119*, 12625–12642.

Table 1 Osmotic pressure, equilibrium hydration states and corresponding equilibrium basal distances, in the vicinity of transitions from one hydration state to another.

P [MPa]	Hydration state Py-Mt:Mt-Mt	d_{PM} [Å]	d_{MM} [Å]
8.4	3WL:3WL	18.8	18.4
14	2WL:3WL	16.4	18.5
16.8	2WL:2WL	16.4	15.8
84	1WL:2WL	12.9	15.2
210	1WL:1WL	12.4	12.7

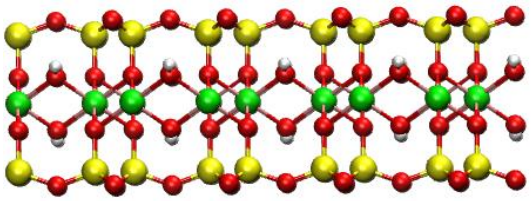

Figure 1 Structure of a pyrophyllite/montmorillonite layer (O: red, H: white, Si: yellow, and Al: green).

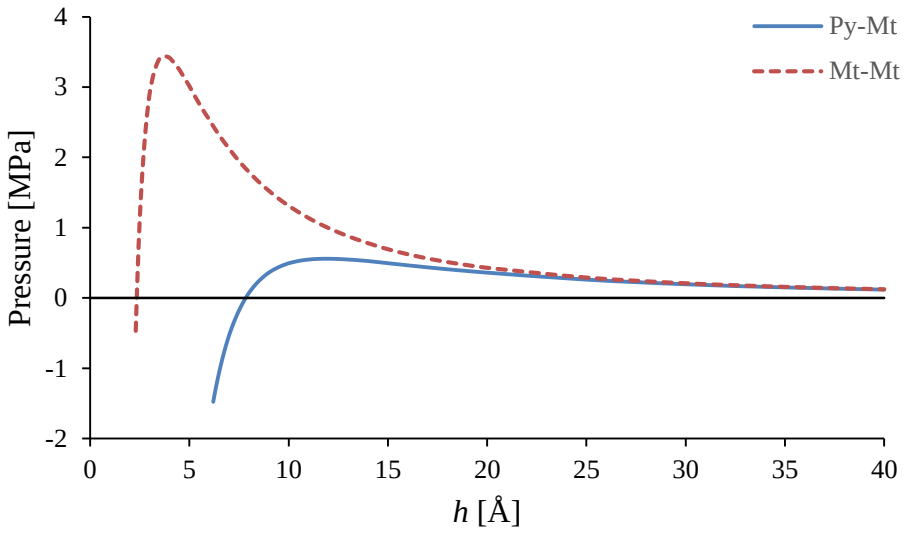

Figure 2 DLVO swelling pressure for Py-Mt and Mt-Mt. As explained in the text, h is the distance from the charged to the neutral surface. Thus the mineral layer separation equals $2h$ for Mt-Mt, while it is h for Py-Mt.

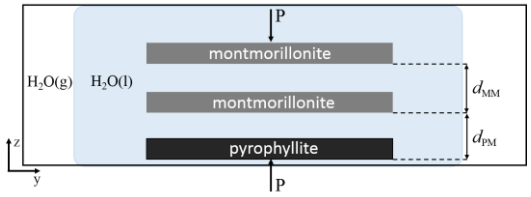

Figure 3 Schematic of the constant load simulation setup. P is the pressure applied to the upper montmorillonite layer and the pyrophyllite layer at the bottom. In between there is a second montmorillonite layer. The simulation cell is large enough that the bulk water is never pressurized but always in equilibrium with vapor.

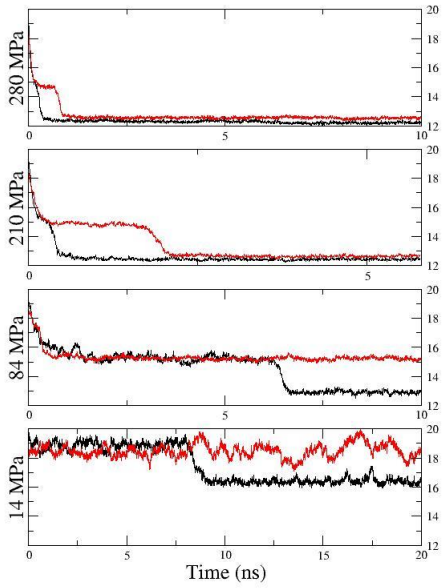

Figure 4 Time evolution of basal distances (y-axis) for four different loads: 14, 84, 210, and 280 MPa. Red lines d_{MM} and black lines d_{PM}.

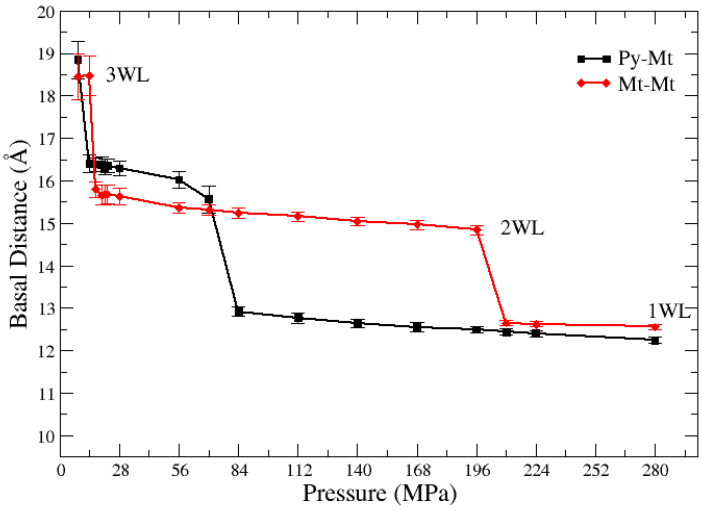

Figure 5 Basal distances as a function of applied pressure (load).

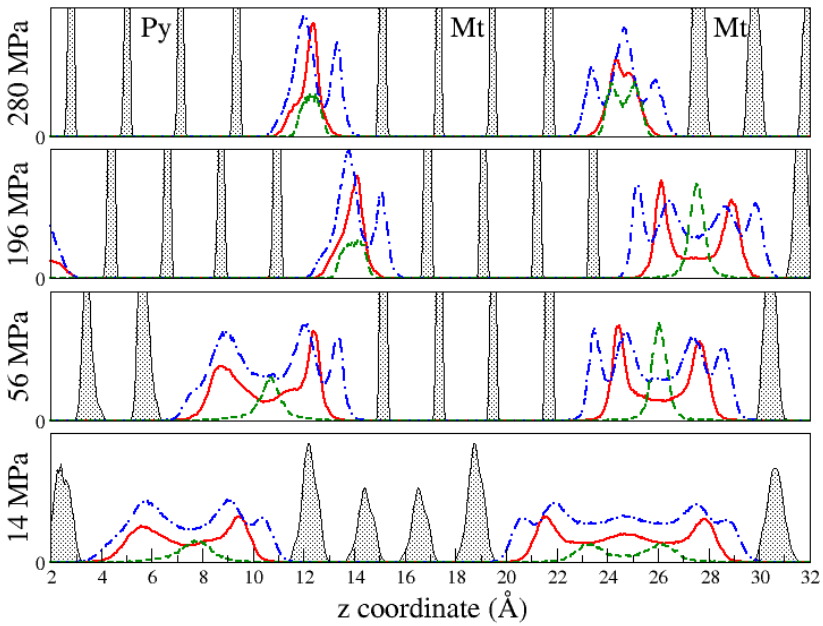

Figure 6 Density profiles of Na^+ (green), water oxygen (red), and water hydrogen (blue) along the *z*-direction. The Na^+ density is enhanced by a factor of five for clarity. Gray shaded peaks are mineral-layer oxygens. All positions are measured relative to the central Mt layer.

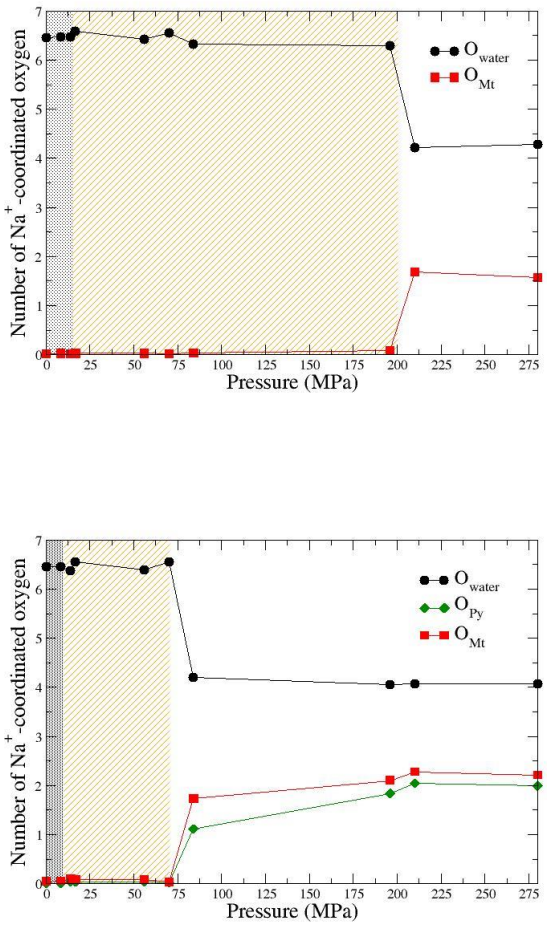

Figure 7 Na^+ coordination number to water and surface oxygens at different applied pressures. Gray shaded, dashed yellow, and white areas refer to 3WL, 2WL, and 1WL, respectively. Upper panel shows Mt-Mt and lower panel Py-Mt interlayer.

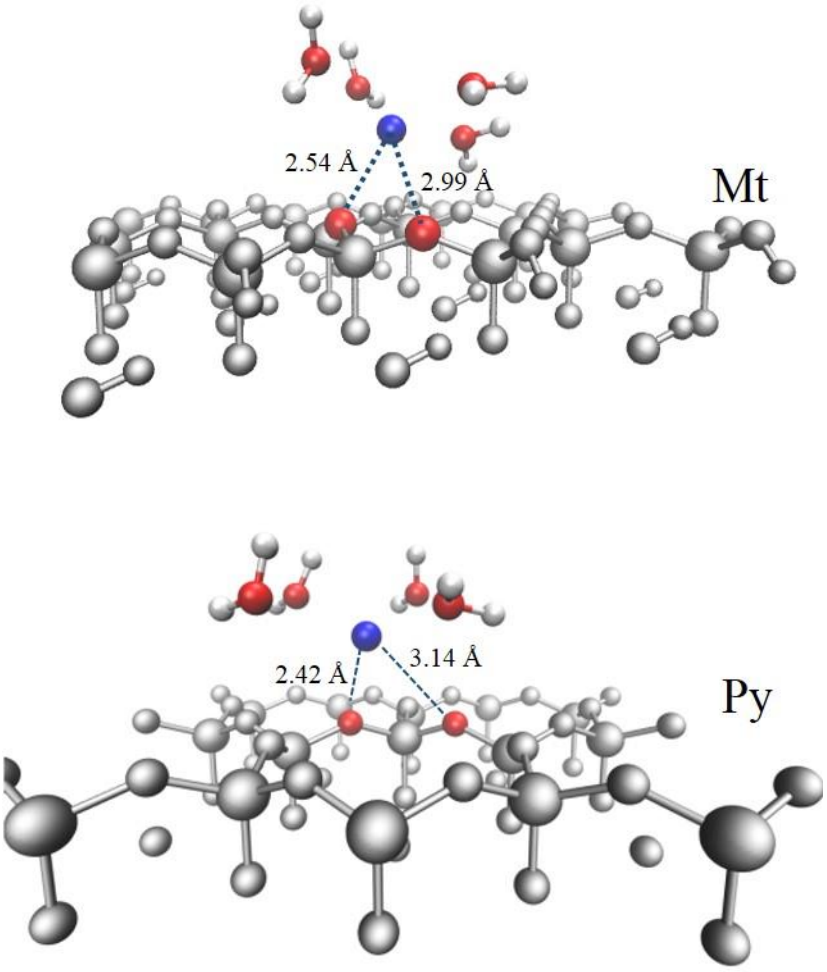

Figure 8 Representative structures for Na^+ coordination near Mt (upper panel) and near Py (lower panel) in the Py-Mt interlayer at 280 MPa.

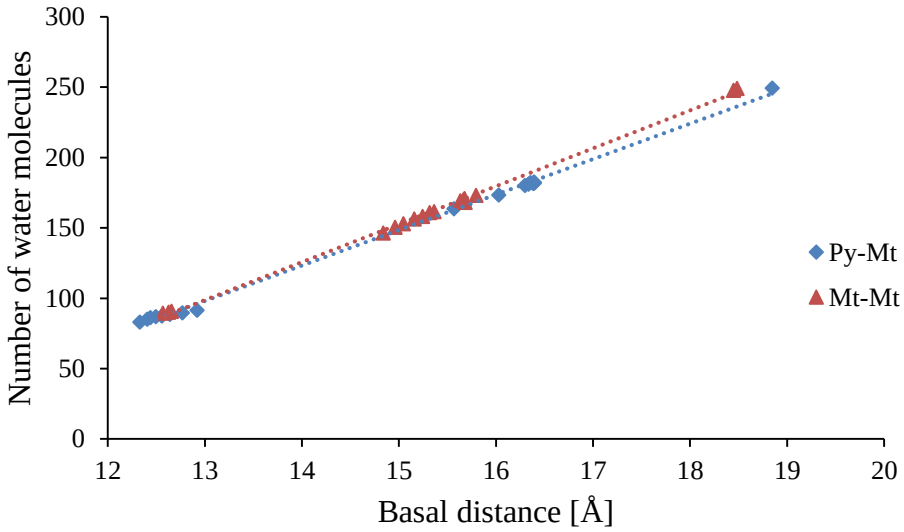

Figure 9 Number of water molecules in the interlayer as a function of average basal distance. Dashed lines are linear regressions to the data points (R^2>0.99).

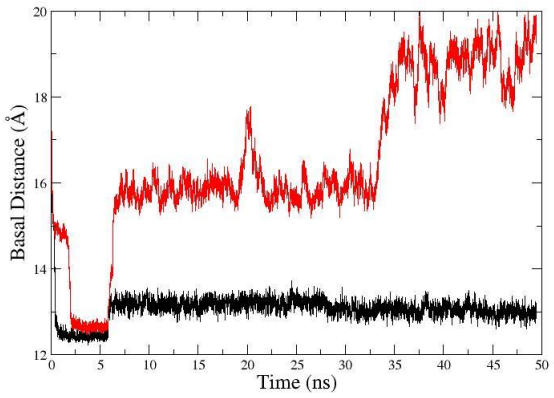

Figure 10 Time evolution of the basal distances d_{PM} (black) and d_{MM} (red). Initially the load was 210 MPa which was reduced to 14 MPa after 6 ns. Mt-Mt expanded, first from 1WL to 2WL and finally to 3WL in response to the reduced load. Py-Mt remained in 1WL during the 50 ns simulation but the interlayer expanded when pressure was reduced to 14 MPa.

TOC Graphic